Heat capacities of freely evaporating charged water clusters

A. E. K. Sundén,[1] K. Støchkel,[2] S. Panja,[2] U. Kadhane,[2] P. Hvelplund,[2] S. Brøndsted Nielsen,[2] H. Zettergren,[2] B. Dynefors,[3] and K. Hansen[1,a)]
[1]*Department of Physics, University of Gothenburg, 41296 Gothenburg, Sweden*
[2]*Department of Physics and Astronomy, University of Aarhus, Ny Munkegade 120, 8000 Aarhus C, Denmark*
[3]*Chalmers University of Technology, 41296 Gothenburg, Sweden*

(Received 17 March 2009; accepted 14 May 2009; published online 12 June 2009)

We report on evaporation studies on positively charged water clusters ($H^+(H_2O)_N$) and negatively charged mixed clusters ($X^-(H_2O)_N$) with a small core ion X ($X=O_2$, CO_3, or NO_3), in the size range $N=5-300$. The clusters were produced by corona discharge in ambient air, accelerated to 50 keV and mass selected by an electromagnet. The loss of monomers during the subsequent 3.4 m free flight was recorded. The average losses are proportional to the clusters' heat capacities and this allowed the determination of size-dependent heat capacities. The values are found to increase almost linearly with clusters size for both species, with a rate of $6k_B-8k_B$ per added molecule. For clusters with $N<21$ the heat capacities per molecule are lower but the incremental increase higher. For $N>21$ the values are intermediate between the bulk liquid and the solid water 0 °C values. © *2009 American Institute of Physics*. [DOI: 10.1063/1.3149784]

I. INTRODUCTION

The ubiquity of water on Earth makes water clusters important objects qua their role as precursors of bulk matter. One place where this role is particularly relevant is in atmospheric nucleation. Although most nucleation in the atmosphere is expected to occur on aerosol particles,[1] the presence of charges in the atmosphere[2] makes ion-induced nucleation a potentially important contributor to total nucleation rates.[3] The thermodynamical properties of water clusters, pure or contaminated, are therefore of relevance for modeling atmospheric processes. In spite of major efforts, both theoretically and experimentally, the determination of thermodynamic properties of water clusters is still lacking compared to the importance of the subject.

Part of the reason for the problems is the broad mass and energy distributions generated in most cluster sources when clusters are studied in the laboratory. Although it is possible to thermalize cluster postproduction, most experiments on medium size and large clusters are performed with molecular beams on these broad precursor distributions. It is, however, possible to use the systematics associated with the broad energy distributions, as done previously for small positively charged water clusters.[4] In this work we will use the assumptions that the clusters have evaporated a molecule at least once after production and entry into vacuum and before size selection in the acceleration stage used here for the mass spectrometry. The degree of metastable decay during free flight after mass selection is proportional to the heat capacity, as will be clear from the derivation presented. Hence measurements of the metastable decay fraction can be inverted to give the heat capacity.

a)Electronic mail: klavs@physics.gu.se.

II. EXPERIMENTAL SETUP AND PROCEDURE

The experiment was carried out in a single pass accelerator which has been described previously in Refs. 5 and 6. The schematic drawing in Fig. 1 gives the parameters that are relevant here.

Water clusters of both positive and negative charge are produced in a corona discharge source[7] at atmospheric pressure (see Ref. 8 for details of the source) and enter vacuum by a 10 cm long (optionally heated) capillary. The high voltage on the STM (scanning tunneling microscope) needle which is used to create the discharge is kept at 2–4 kV, depending on the desired cluster size distribution. To optimize the intensity when smaller cluster sizes are of interest, the capillary is heated slightly above room temperature, up to 60 °C (see Fig. 2).

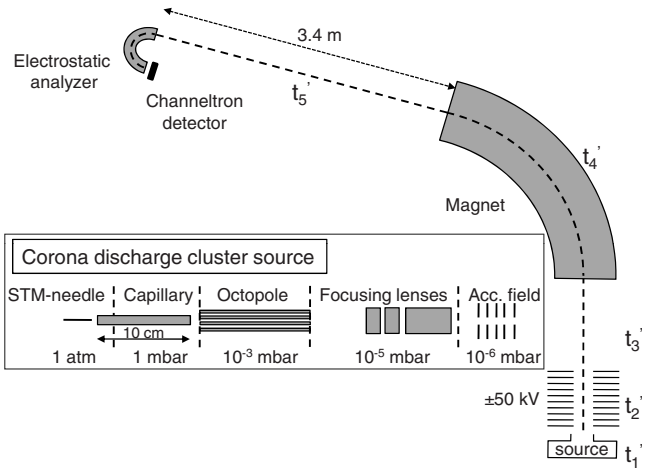

FIG. 1. The experimental setup. Clusters are produced in a corona discharge in ambient air and enter the chamber through the capillary. The inset shows a magnified view of the corona discharge source, turned 90° clockwise. The large figure shows the entire apparatus with the free flight distance at 3.4 m indicated. The t_n's in the figure are explained in the text.

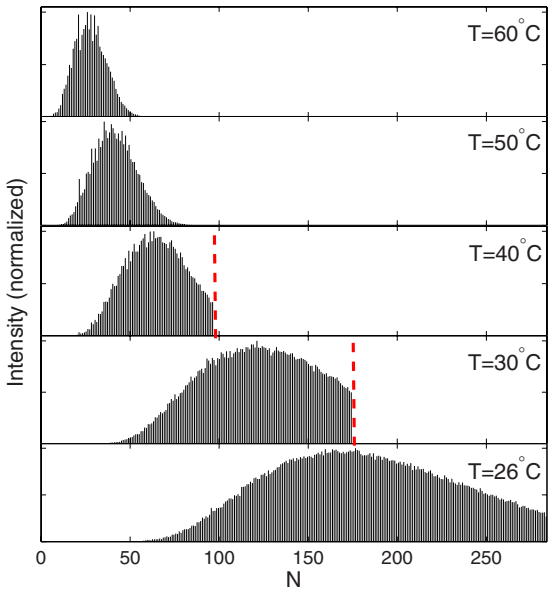

FIG. 2. (Color online) Cluster size distribution of $H^+(H_2O)_N$ obtained by scanning the field in the magnet. The maximum intensity for the distributions shifts toward larger cluster sizes with decreasing temperature of the capillary. The scans at $T=40$, 30, and 26 °C where terminated at the masses indicated by the vertical bars. Individual mass peaks have been integrated and the spectra normalized to the highest intensity in each spectrum. The ion intensity variations are related to the stability of specific clusters and not caused by poor statistics.

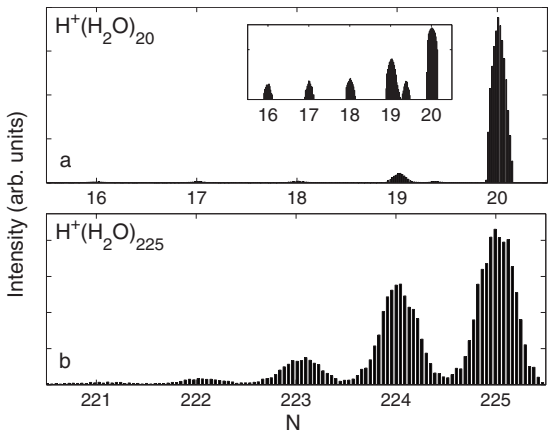

FIG. 3. Evaporation spectra of the parent cluster $H^+(H_2O)_{20}$ in (a) and $H^+(H_2O)_{225}$ in (b). The peaks showing loss of multiple molecules in (a) are used to correct for CID. The inset here and in Fig. 4 is a semilogarithmic plot of the data.

The beam is guided using an octopole and a set of electrostatic lenses after which they are accelerated to typically 50 keV. After acceleration the cluster mass of interest is selected in the electromagnet and after a 3.37 m long free flight the clusters are detected using a hemispherical electrostatic analyzer.[9]

The cluster charge is changed between positive and negative by switching polarity on the needle and the concomitant changes in the ion optics, acceleration, etc. The positively charged clusters are predominantly pure protonated water clusters, $H^+(H_2O)_N$ with a small admixture of ammonia containing clusters, $(NH_4^+(H_2O)_N)$. Since the mass of NH_4^+ is 1 Da less than that of H_3O^+, ammonia-mixed clusters can be separated out and excluded from the experiments. When studying the negatively charged clusters we see no pure water clusters. Instead they contain a negative core ion. The core ion has been identified in experiments with collision induced dissociation (CID) for the data points $N=10-14$ performed with the same source and mass spectrometer to be O_2^-. Above $N=18$ cluster masses indicate core ions of CO_3^-. Other core ions like $NO_3^-(HNO_3)_n$ have been identified previously,[10] with an appearance that depend on the precise source conditions.

The times spent by the clusters in the different sections of the experimental apparatus are important as will be clear below. For a charged particle the times depend on the mass, distances, and electrostatic potentials. In addition, the ions have a small energy associated with the initial speed acquired in the expansion into vacuum. We used the speed of 330 m/s, corresponding to 0.01 eV per water molecule and a Mach number slightly above one. Figure 1 shows the breakdown of the ion flight through the apparatus into sections of relevance for the analysis. For a cluster of $N=50$ molecules the times are $t_1'=68$ μs (from entry into vacuum until acceleration), $t_2'=10$ μs (acceleration time), $t_3'=11$ μs (free flight between acceleration and mass selection in magnet), $t_4'=25$ μs (magnet transit time), and $t_5'=36$ μs (free flight). These times scale approximately with $\sqrt{m}$, but not exactly because of the small size-dependent initial energy.

III. RESULTS

Figure 2 shows examples of cluster size distributions obtained by scanning the magnetic field for different capillary temperatures. Care has been taken to correct for several factors which may distort the signal. The increased fragmentation due to rest gas collisions (CID) in the free flight zone was corrected by fitting the fragment peaks that cannot originate from spontaneous evaporation and subtract these extrapolated intensities from the measured daughter peaks. The number of fragment peaks used for this procedure changes with precursor size. For clusters with $N<60$ one daughter peak was counted as true evaporation; for $60<N<160$ the number was two and for $160<N<300$ three daughter peaks where included in the analysis. The corrections from rest gas collisions are in all cases minor. The metastable evaporation for $N=20$ and $N=225$ is shown in Figs. 3 and 4.

For $N\geq 10$, $H^+(H_2O)_{N+1}$ fragmenting into $H^+(H_2O)_N$ in the field free region before mass selection will give a spurious contribution to the $H^+(H_2O)_{N-1}$ signal in the electrostatic analyzer.[11] However, in the size region $10<N<23$ the two peaks can be resolved and the ratio of the contribution from $H^+(H_2O)_{N+1}$ was determined to be $\approx 10\%$ of the first daughter peak and 10% of the counts in the first daughter peak are therefore subtracted for $N>23$. The same procedure was used to correct the anion spectra.

The corrected relative intensities of the parent cluster and the fragments are plotted in Fig. 5. The amount of unevaporated parent cluster decreases rather smoothly as the size increase. This is mirrored in the smooth increase in first the singly evaporated species and at larger sizes the doubly evaporated clusters. There is little difference between the behavior of the positive and negative clusters although the an-

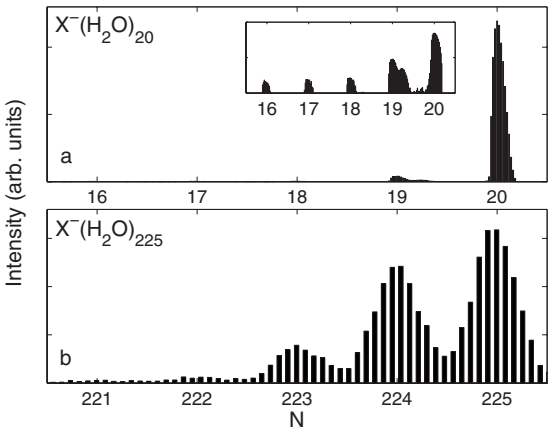

FIG. 4. Evaporation spectra of the parent cluster $X^-(H_2O)_{20}$ in (a) and $X^-(H_2O)_{225}$ in (b). X is most likely CO_3 for $N=20$ and O_2 for $N=225$.

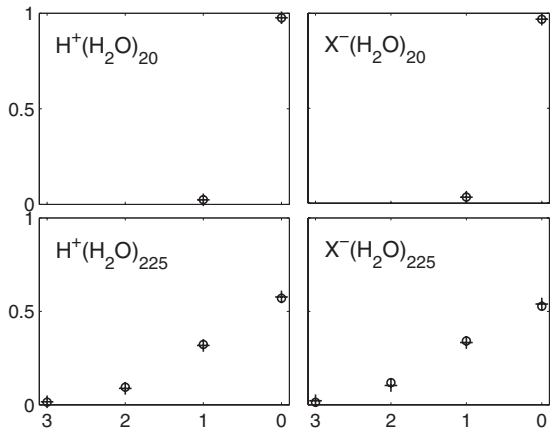

FIG. 6. Example of integrated and corrected abundances (○) and the fit using the Poisson distribution (+) for both positive $(H^+(H_2O)_N)$ and negative $(X^-(H_2O)_N)$ clusters with $N=20$ and 225.

ions tend to evaporate slightly more for a given cluster size. The trend with increasing evaporation as a function of size is expected for the evaporative ensemble and reflects the increase in heat capacity with size.[12] The only anomaly in our data is the negative ion points for $N=70-77$. Although we suspect the quality of these specific data points we have chosen to include them in the analysis.

IV. ANALYSIS

As already indicated Fig. 5 shows that the decay process is occurring with increasing probability the larger the cluster. For a sequential process one may attempt to approximate the number of evaporated molecules with a Poisson distribution, considering the evaporation events as independent and happening with the same rate constant for all decay from a given precursor size. This turns out a fairly good approximation. Figure 6 shows the measured, integrated peak intensities for the cluster sizes shown in Figs. 3 and 4. For the large clusters one sees a very small deviation from Poisson distributions. Although small it is nevertheless statistically significant. A slightly more well defined quantity than the fitted mean value of a Poisson distribution is the probability for the cluster to survive the free flight, P. For Poisson distributions, this is related to the mean number of lost monomers, λ, as $P=\exp(-\lambda)$. As shown in Fig. 7 for both charge states and $N=5-300$, the two are very similar. The other noteworthy feature of the curve is the quite remarkable proportionality between the average molecule loss and size. We will use the P's in the subsequent analysis because they are insensitive to the corrections that must be made to the Poisson distribution for a more realistic description of the decay dynamics.

A note on the accuracy of the Poisson distribution is in place. By approximating the number of evaporated molecules with a Poisson distribution one assumes that all decays have identical rate constants. This is only correct in the limit where consecutive decay rate constants are identical, e.g., if dissociation energies and temperatures of the clusters do not depend on the length of the decay chain. This holds to a good approximation for large clusters, because the large heat capacity yields almost identical microcanonical temperatures for $N-1$ produced by decay from N, and also because the binding energies tend to vary only slowly with size in this limit. These conditions cannot be expected to hold for small sizes, in general, but in this limit the Poisson distribution is nevertheless a good approximation because the number of evaporated molecules is small and a second evaporation, where the problem shows up, is exceedingly rare.

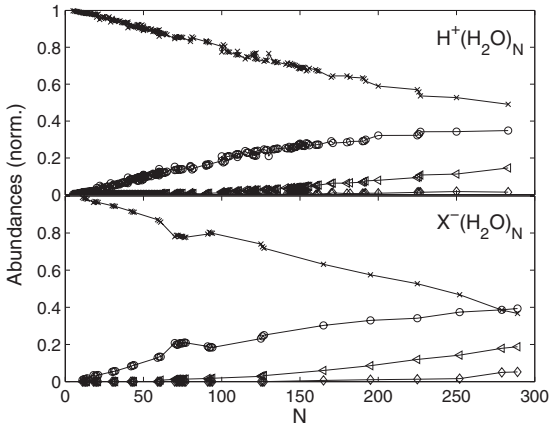

FIG. 5. Normalized abundances after free flight where the symbols represent undissociated parent clusters (×), singly dissociated (○), doubly dissociated (◁), and triply dissociated clusters (◇).

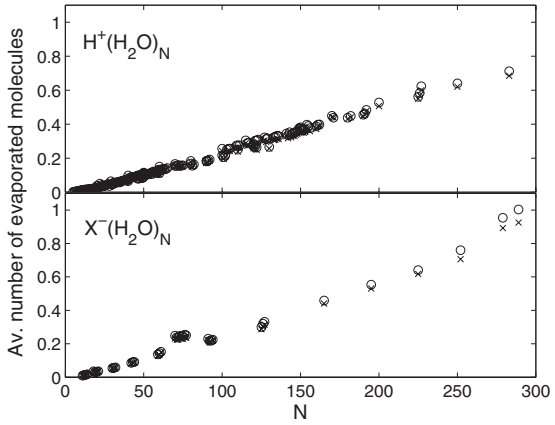

FIG. 7. Test of the approximation to use P (the surviving fractions of the parent clusters) to represent the distribution of average number of water molecules lost. The λ's obtained by using either the whole evaporation spectrum (×) or calculated as $-\ln(P)$ (○).

Because the Poisson distribution can be expected to hold in both the small and the large size limits, it can be used for intermediate sizes with good results, as demonstrated in Fig. 7.

The connection between the decay rates and the heat capacity appears in the systematics of the evaporative ensemble. The water clusters are created hot and cool down by evaporation. In the theory, internal energy (or temperature) distributions depend on the dissociation energies.[12] The energy distributions also depend on size, or specifically the heat capacity, of the clusters. Heat capacities below the critical value $(\ln(\omega t))^2$, where t is the measurement time and ω the frequency factor in the unimolecular evaporation rate constant, will have an approximately square distribution with a width close to the dissociation energy D. For clusters above this size the energy distributions will have a Gaussian shape with a narrow temperature distribution.[13] The consequence of this is that the metastable evaporation originates from depletion of the high energy side of the energy distribution for small, free clusters, and from homogeneous depletion simultaneous across the whole energy distribution for large clusters. These two situations will therefore need to be treated separately. For a more detailed discussion of the shape of these distributions and their consequence for evaporative ensemble observables, please consult Refs. 12 and 13.

We will approximate rate constants with Arrhenius expressions, $k=\omega \exp(-D/T)$, where D is the approximately size independent dissociation energy. The temperature T used in this expression is the microcanonical temperature of the parent, modified with the finite heat bath correction $-D/2C_{v,N}$ where $C_{v,N}$ is the heat capacity (we set Boltzmann's constant k_B to one. A heat capacity of one corresponds to 0.0862 meV/K). Alternatively it is the daughter temperature with a correction of $+D/2C_{v,N}$. For a detailed discussion of the use of temperatures for microcanonical rate constants, see, e.g., Refs. 14 and 15. Although the heat capacity enters here, it will only appear in an additive term which is constant to a good approximation in the intervals we consider here. The change in effective temperature upon one evaporation is therefore $\Delta T=D/C_{v,N}$, disregarding the small kinetic energy release, and corrections of similar magnitude.

The frequency factor ω in the rate constant can be calculated from detailed balance considerations.[16] The value depends on cluster size as well as temperature, but these are weak dependencies compared with the Boltzmann factor in the Arrhenius formula. The size dependence enters the frequency factor through the capture cross section of the inverse process. Data on sticking of water molecules to water clusters give no indication that the cross section is significantly lower than the geometric, using the bulk density of water.[17,18] For a product temperature of $T=150$ K the values are $\omega = 6.33\times 10^{16} N^{2/3}$ s^{-1}. This expression is based on a transition state corresponding to the asymptotically separated fragments, and includes the translational, vibrational, and rotational degrees of freedom of the water molecule.

A. Large cluster evaporation statistics

The evaporation rate can be written as[12]

$$R = c\frac{C_{v,N}}{(\ln(\omega t))^2}\frac{1}{t}, \tag{1}$$

where t is the time since the creation of the ensemble, i.e., the entry into vacuum, and c is a constant which is determined by the ion beam intensity. For large clusters, Eq. (1) also gives the decay rate constant, which is identical for all ions in the ensemble;

$$k_N = \frac{C_{v,N}}{(\ln(\omega t))^2}\frac{1}{t}. \tag{2}$$

The fact that all ions have the same decay constant means that the time that should be used in the expression is the latest time for which decays are nondestructive, or in other words the latest time for which the decay of size N feeds the size $N-1$. Here, this time is equal to the time from entry into vacuum to initial acceleration. If we for future use define the accumulated times as

$$t_j = \sum_{i=1}^{j} t_i', \tag{3}$$

the mass selection time is equal to t_1. Upon entry of the electrostatic analyzer we therefore have a surviving fraction of

$$P = e^{-k(t_1)t_5'} = \exp\left(-\frac{C_{v,N}}{(\ln(\omega t_1))^2}\frac{t_5'}{t_1}\right). \tag{4}$$

Equation (4) can be rearranged to give us the heat capacity $C_{v,N}$ per cluster:

$$C_{v,N} = \frac{-\ln(P)}{t_5'/t_1}(\ln(\omega t_1))^2. \tag{5}$$

B. Small cluster evaporation statistics

For small clusters the decrease of the highest energy part of the cluster population differs strongly from that of the lowest energy population. The highest excitation energy at any given time is given by $E_{\max,N}=DC_{v,N}/\ln\ \omega t+E_0$, and the decrease during free flight from time t_4 to t_5 is then

$$\Delta E = E_{\max}(t_4) - E_{\max}(t_5) \approx D\frac{C_{v,N}\ln(t_5/t_4)}{(\ln(\omega t_4))^2}. \tag{6}$$

The energy distribution has a width of D at t_1 and to get the proper normalization of the decay probability we need to take in account the depletion caused by the decay from t_1 to t_4. The situation is illustrated in Fig. 8. The result is the survival probability

$$P \approx \left(1-\frac{C_{v,N}\ln(t_5/t_1)}{(\ln(\omega t_4))^2}\right)\left(1-\frac{C_{v,N}\ln(t_4/t_1)}{(\ln(\omega t_4))^2}\right)^{-1}. \tag{7}$$

Solving for $C_{v,N}$ we have

$$C_{v,N} \approx \frac{1-P}{\ln(t_5/t_1)-P\ln(t_4/t_1)}(\ln(\omega t_4))^2. \tag{8}$$

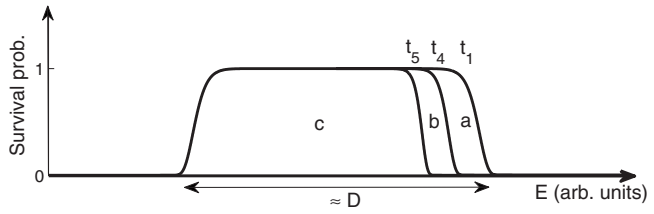

FIG. 8. A schematic drawing of the energy distribution of the small cluster ensemble. The clusters are depleted from the high energy side of the energy distribution. The times t_1, t_4, t_5 refer to the different times of passage in the apparatus.

V. DISCUSSION

The expected crossover from large to small clusters and hence from the values given by Eq. (8) to those of Eq. (5) are $C_{v,N} \simeq (\ln(\omega t_4))^2 = 1086$ (for t_4 corresponding to $N=160$). The $C_{v,N}$'s calculated from the data for the two limits cross close to this value, at $C_{v,N} \approx 850$, $N=170$ for the positively and $C_{v,N} \approx 800$, $N=140$ for the negatively charged clusters. We have therefore used the small cluster limit below these sizes and the large cluster limit above.

The final result of the analysis is plotted in Fig. 9 for both positive and negative clusters. For reference, the heat capacities for bulk ice and liquid water at a few different temperatures are also plotted. The inset shows the small-to-medium size cluster region. Note that size-to-size variations should be disregarded because the procedure assumes similar dissociation energies for parent and daughter cluster and the normalization reflects this. The error bars represent the reproducibility of repeated measurements. We have estimated the effect of the uncertainty of the atmosphere-to-vacuum expansion speed by calculating heat capacities with the speeds 0.5×330 and 1.5×330 m/s. The results were changes in the heat capacity of about 1% for the smallest clusters up to 9% for $N=300$.

The dominant feature in the curve is the almost linear increase with size for both negatively and positively charged clusters. Roughly speaking the heat capacity increases with $6k_B - 8k_B$ per added molecule. This corresponds approximately to a harmonic oscillator heat capacity of the six external degrees of freedom of the water molecule, indicating that the intramolecular vibrations are still frozen. In addition to these frozen degrees of freedom, the overall rotational and translational degrees of freedom do not contribute to the measured heat capacity. This reduces the number of vibrational degrees of freedom with 6, which corresponds to the contribution of a single water molecule as judged from the slope of the experimental curve. The experimental curve extrapolates to zero heat capacity at $N \approx 5$ for the positively charged and slightly higher for the negatively charged. One reason for this is that the approximations leading to the Arrhenius expression for the evaporative rate constant fails for small heat capacities.[14]

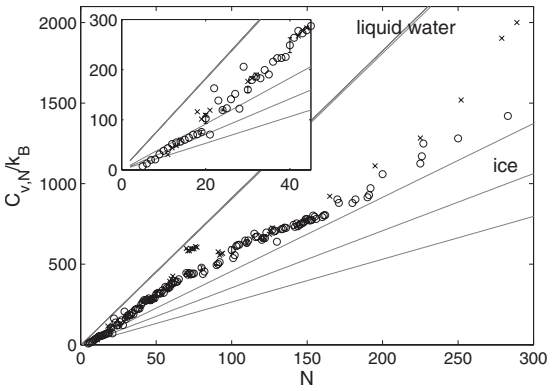

FIG. 9. The dimensionless heat capacities for positively (○) and negatively charged clusters (×). The lines are given for reference and represent literature values for bulk ice [at $P=1$ atm and $T=0$ °C (topmost ice line), −63 °C (middle line), and −123 °C (bottom line, from Ref. 19) and for bulk liquid water (at $P=1$ atm and $T=0$, 50, and 100 °C, from Ref. 20). The liquid water lines almost coincide.

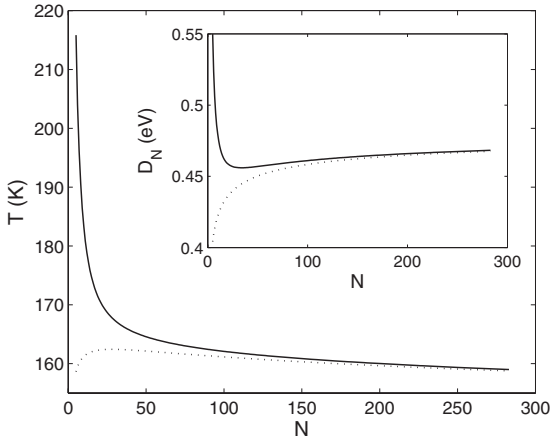

FIG. 10. The temperature T_N calculated using dissociation energies D_N from the liquid drop model and the relation $D_N/T = \ln(\omega t)$. The solid line includes the cohesive energy, surface tension, and charge energy. The dotted line represents the calculated T_N when the charge effect is neglected. Sizes down to $N=5$ are plotted. The inset shows the dissociation energy D_N used for the calculation, with and without the charging energy included.

The slope of the curves $C_{v,N}$ versus N changes slightly but discernibly around $N=20$. We expect that this is associated with the completion of a geometric shell. For the positively charged clusters there is a well-known "magic number" at $N=21$ whereas the picture for the negatively charged is different.

The second important feature in the data is that there is only a small difference between the positively and the negatively charged clusters. This is not surprising given the cluster sizes studied here. For medium size and large clusters we do not expect that the charge will influence the thermal properties significantly.

The heat capacities measured pertain to the temperatures reached in an ensemble of freely evaporating clusters in vacuum. The energy could possibly equilibrate by absorption and emission of infrared radiation, but this process is slow compared with the transit time and can be ignored here.[21] We can therefore estimate the temperatures of the clusters with the evaporative ensemble values. The details of this calculation are given in Appendix. The results are based on the liquid drop expansion of the energy, taking into account the bulk cohesive energy, the surface tension, and the charging energy. The calculated dissociation energies and ensemble temperatures are shown in Fig. 10. Except for the very smallest sizes, the temperature is around 160 K. This value is

robust for very large clusters that are certainly icelike with a corresponding icelike heat capacity. At smaller sizes the melting point depression for small clusters could potentially reach the evaporative ensemble temperatures here. In this connection it is of interest to note the early observation[22] that magic numbers associated with a solidlike state requires several microseconds to appear in the mass spectra. A melting point depression would tend to increase the heat capacity to the liquid water value but this seems not to happen here, although cluster sizes around $N=100$ have a somewhat elevated heat capacity. This trend is reversed for smaller sizes. We tentatively ascribe this reversal to the effect of the charge. We expect that the presence of a net charge is important for water clusters because of the large water monomer dipole moment. A detailed treatment of this phenomenon is beyond the scope of this article.

Hock *et al.*[23] measured heat capacities with a temperature-resolved method for the clusters $(H_2O)_{48}^-$ and $(H_2O)_{118}^-$. The data suggest a lower value for the two cases than our results but also refer to slightly lower temperatures. Extrapolation of their data appears consistent with our temperatures-heat capacities, indicating that the suggested liquid drop parameterization of the binding energy is reasonable.

ACKNOWLEDGMENTS

This work has been supported by the Swedish National Research Council (VR), the University of Gothenburg Nanoparticle platform, and the EU-project ITSLEIF.

APPENDIX: LIQUID DROP MODEL DISSOCIATION ENERGIES AND CLUSTER TEMPERATURES

The measurements do not contain direct information about the cluster temperatures. We can estimates these as a certain fraction of the dissociation energies D_N, for which we use the liquid drop expansion. Although this is often used for metal clusters it has also been applied to water clusters in, e.g., Ref. 4 where Gibbs' free energy differences are calculated in a liquid drop expansion. We will use the model for charged cluster dissociation energies as opposed to cluster enthalpies or free energies. The ground state energy differences are likely to be most relevant because the microcanonical rate constants involve these differences, and not differences in, e.g., enthalpies. We emphasize that the numbers derived are only estimates but feel that the estimates are warranted because of the good agreement with the data of Ref. 23.

The monomer dissociation energy for a charged cluster can be approximated as

$$D_N \approx A - \frac{2B}{3}N^{-1/3} + CN^{-4/3}, \tag{A1}$$

where A is the bulk cohesive energy per molecule, B is the surface energy term which is $B=4\pi r_1^2\sigma_s$, and C is the charging energy term equal to[4,24]

$$C = \frac{1}{2}\frac{e^2}{4\pi\epsilon_0}\left(1-\frac{1}{K}\right)\frac{1}{r_1}\frac{1}{3}. \tag{A2}$$

The value of A is 0.49 eV, compared to a 0 °C liquid water enthalpy of vaporization of 0.47 eV.[25] To calculate B we need r_1 for which we use the bulk liquid water density, also at 0 °C, which gives $r_1=1.92$ Å. The surface tension σ_s is 75.64 mJ/m^2 for liquid water at $T=0.01$ °C.[26] The relative dielectric constant K is temperature dependent. In the case of liquid water it ranges from 55 to 88,[27] and in ice it ranges from around 90 to 200.[28] These high values allows us to approximate $1/K$ with 0 in Eq. (A2).

In summary, we have the values $A=0.49$ eV, $B=0.22$ eV, and $C=1.25$ eV. In Fig. 10 the dissociation energy is calculated using the liquid drop model, with and without inclusion of the charging energy. To calculate an approximative cluster temperature we have the evaporative ensemble relation

$$\frac{D_N}{T_{\max}} = \ln(\omega t_1), \tag{A3}$$

where ω is the Arrhenius frequency factor, equal to $\omega=6.33\times10^{16}N^{2/3}$ s^{-1} and t_1 is the time from creation to mass selection. Solving for T gives us Fig. 10. The temperature calculated is the average of the microcanonical temperatures of the parent and the product cluster, of the hottest clusters in the ensemble around the time t_1.

[1] D. A. Hegg and M. B. Baker, Rep. Prog. Phys. **72**, 056801 (2009).
[2] R. P. Wayne, *Chemistry of the Atmosphere* (Oxford University Press, Oxford, 2000).
[3] M. B. Enghoff, P. O. P. Pedersen, T. Bondo, M. S. Johnson, S. Paling, and H. Svensmark, J. Phys. Chem. A **112**, 10305 (2008).
[4] Z. Shi, J. V. Ford, S. Wei, and A. W. Castleman, Jr., J. Chem. Phys. **99**, 8009 (1993).
[5] P. Hvelplund, L. H. Andersen, H. K. Haugen, J. Lindhard, D. C. Lorents, R. Malhotra, and R. Ruoff, Phys. Rev. Lett. **69**, 1915 (1992).
[6] P. Hvelplund, L.H. Andersen, C. Brink, D.H. Yu, D.C. Lorents, and R. Ruoff, Z. Phys. D: At., Mol. Clusters **30**, 323 (1994).
[7] M. Tsuchiya, K. Otsuka, and H. Kuwabara, Chem. Lett. **1985**, 709 (1985).
[8] O. V. Boltalina, P. Hvelplund, T. J. D. Jørgensen, M. C. Larsson, and D. A. Sharoitchenko, Phys. Rev. A **62**, 023202 (2000).
[9] H. Shen, P. Hvelplund, D. Mathur, A. Bárány, H. Cederquist, N. Selberg, and D. C. Lorents, Phys. Rev. A **52**, 3847 (1995).
[10] K. Drenck, P. Hvelplund, S. Brøndsted Nielsen, S. Panja, and K. Støchkel, Int. J. Mass Spectrom. **273**, 126 (2008).
[11] D. Schröder and D. Sülze, J. Chem. Phys. **94**, 6933 (1991).
[12] K. Hansen and U. Näher, Phys. Rev. A **60**, 1240 (1999).
[13] U. Näher and K. Hansen, J. Chem. Phys. **101**, 5367 (1994).
[14] C. E. Klots, Z. Phys. D: At., Mol. Clusters **20**, 105 (1991).
[15] J. U. Andersen, E. Bonderup, and K. Hansen, J. Chem. Phys. **114**, 6518 (2001).
[16] K. Hansen, Philos. Mag. B **79**, 1413 (1999).
[17] F. Chirot, P. Labastie, S. Zamith, and J. M. L'Hermite, Phys. Rev. Lett. **99**, 193401 (2007).
[18] J. M. L'Hermite, private communication (November 2008).
[19] D. M. Murphy and T. Koop, Q. J. R. Meteorol. Soc. **131**, 1539 (2005).
[20] *CRC Handbook of Chemistry and Physics*, 58th ed. (CRC, Boca Raton, 1978).
[21] T. Schindler, C. Berg, G. Niedner-Schatteburg, and V. E. Bondybey, Chem. Phys. Lett. **250**, 301 (1996).
[22] O. Echt, D. Kreisle, M. Knapp, and E. Recknagel, Chem. Phys. Lett. **108**, 401 (1984).

[23] C. Hock, M. Schmidt, R. Kuhnen, C. Bertels, L. Ma, H. Haberland, and B. v. Issenddorff, "Calorimetric observation of the melting of free water nanoparticles at cryogenic temperatures" (submitted).
[24] K. Hansen and E. E. B. Campbell, Int. J. Mass Spectrom. **233**, 215 (2004).
[25] *CRC Handbook of Chemistry and Physics*, 89th ed. (CRC, Boca Raton, 2008).
[26] J. R. Cooper, IAPWS Release on Surface Tension of Ordinary Water Substances, International Association for the Properties of Water and Steam, 1994.
[27] C. G. Malmberg, and A. A. Maryott, J. Res. Natl. Bur. Stand. **56**, 1 (1956).
[28] M. E. Hobbs, M. S. Jhon, and H. Eyring, Proc. Natl. Acad. Sci. U.S.A. **56**, 31 (1966).